Organs-on-a-Chip 3 (2021) 100010

Contents lists available at ScienceDirect

Organs-on-a-Chip

journal homepage: www.sciencedirect.com/journal/organs-on-a-chip

In vitro nonalcoholic fatty liver disease model with cyclo-olefin-polymer-based microphysiological systems

Xiaopeng Wen [a,1], Koki Yoshimoto [a,b,c,1], Makoto Yamanaka [d], Shiho Terada [a], Ken-ichiro Kamei [a,e,f,*]

[a] Institute for Integrated Cell-Material Sciences (WPI-iCeMS), Kyoto University, Yoshida-Ushinomiya-cho, Sakyo-ku, Kyoto, 606-8501, Japan
[b] Department of Biosystems Science, Institute for Frontier Life and Medical Sciences, Kyoto University, Shogoin-Kawara-cho, Sakyo-ku, Kyoto, 606-8397, Japan
[c] Laboratory of Cellular and Molecular Biomechanics, Graduate School of Biostudies, Kyoto University, Yoshida-Konoe-cho, Sakyo-ku, Kyoto, 606-8397, Japan
[d] Incubation Center Organs on Chip Project, Ushio INC, 1-6-5 Marunouchi, Chiyoda-ku, Tokyo, 100-8150, Japan
[e] Wuya College of Innovation, Shenyang Pharmaceutical University, Liaoning, 110016, People's Republic of China
[f] Department of Pharmaceutics, Shenyang Pharmaceutical University, Liaoning, 110016, People's Republic of China

ARTICLE INFO

Keywords:
Nonalcoholic fatty liver disease
In vitro disease model
Cyclo-olefin polymer
Polydimethylsiloxane
Microphysiological system

ABSTRACT

Nonalcoholic fatty liver disease (NAFLD) is one of the most common chronic liver conditions, and its treatment involves curing the patients without liver transplantation. Understanding the mechanism of NAFLD initiation and progression would enable the development of new diagnostic tools and drugs; however, until now, the underlying mechanisms of this condition remain largely unknown owing to the lack of experimental settings that can simplify the complicated NAFLD process *in vitro*. Microphysiological systems (MPSs) have long been used to recapture human pathophysiological conditions *in vitro* for applications in drug discovery. However, polydimethylsiloxane (PDMS) is used in most of these MPSs as the structural material; it absorbs hydrophobic molecules, such as free fatty acids (FFAs), which are the key components that initiate NAFLD. Therefore, the current PDMS-based MPSs cannot be directly applied to *in vitro* NAFLD modeling. In this work, we present an *in vitro* NAFLD model with an MPS made of cyclo-olefin polymer (COP), namely COP-MPS, to prevent absorption of FFAs. We demonstrated the induction of NAFLD-like phenotype in HepaRG hepatocyte-like cells cultured in the COP-MPS by treatment with FFAs. The FFAs induced lipid accumulation in the HepaRG cells, resulting in inactivation of the apoptotic cells. We believe that the proposed COP-MPS can contribute toward the investigation of NAFLD mechanisms and identification of new drugs to prevent the progression of liver disease and thus avoid liver transplantation.

1. Introduction

Nonalcoholic fatty liver disease (NAFLD) is a common chronic liver condition associated with metabolic syndrome, such as obesity, hypertension, hyperlipidemia, cardiovascular dysfunction, systemic inflammation, and many extrahepatic diseases (Younossi, 2019; Byrne and Targher, 2015; Younossi et al., 2019). Liver transplantation is still the only means of preventing the progression of and curing liver diseases, but it is extremely difficult to match donors to patients. Therefore, there is an urgent need to find alternative means to cure patients. NAFLD is one of the critical stages in the progression of liver diseases. However, it is a complex disease that encompasses a broad spectrum of hepatic phenotypes, including nonalcoholic steatohepatitis, liver fibrosis, and inflammation (Tilg et al., 2020), and the underlying mechanisms of NAFLD progression are still largely unknown. Thus, there are no effective treatments and drugs to cure patients with NAFLD.

To elucidate the mechanisms of NAFLD progression, experimental models such as animal models (Liu et al., 2013) and *in vitro* human

Abbreviations: NAFLD, Nonalcoholic fatty liver disease; MPS, microphysiological system; PDMS, polydimethylsiloxane; FFA, free fatty acid; COP, cyclo-olefin polymer; PS, Polystyrene; PMMA, polymethyl methacrylate; PP, polypropylene; VUV, vacuum ultraviolet; PA, palmitic acid; OA, oleic acid; hiPSC, human induced pluripotent stem cell.

* Corresponding author. Institute for Integrated Cell-Material Sciences (WPI-iCeMS), Kyoto University, Yoshida-Ushinomiya-cho, Sakyo-ku, Kyoto, 606-8501, Japan.
E-mail address: kamei.kenichiro.7r@kyoto-u.ac.jp (K.-i. Kamei).
[1] These authors have contributed equally.

https://doi.org/10.1016/j.ooc.2021.100010
Received 28 December 2020; Received in revised form 11 October 2021; Accepted 5 November 2021
Available online 8 November 2021

models (Boeckmans et al., 2018; Davidson et al., 2016) have been used in literature. Animal models allow addressing the mechanism of NAFLD progression *in vivo*; however, differences in species cannot be ignored. On the other hand, *in vitro* human models using human primary hepatocytes or cell lines have been used to simplify NAFLD for better understanding and application to drug screening. Further, most cell culture methods that are currently used involve cell culture plates and flasks, which cannot represent the *in vivo* physiological conditions, thus resulting in less functionality of the cultured hepatocytes.

To address these issues, microphysiological systems (MPSs) or organ/body-on-a-chip systems based on microfluidic technology offer the possibility of simulating human physiological and pathological conditions *in vitro* for application in drug development, toxicological tests, and disease modeling (Kimura et al., 2018; Benam et al., 2015; Sung et al., 2019; Soto-Gutierrez et al., 2017; Kamei et al., 2017). MPS platforms provide dynamic and three-dimensional culture conditions that are unavailable in conventional cell culture methods to improve cellular functions. However, MPS platforms still have some issues to be addressed, particularly those based on polydimethylsiloxane (PDMS), which has often been used in the fabrication of MPS platforms owing to its biocompatibility, gas permeability, and transparency. Because PDMS also exhibits hydrophobicity and porosity, which allows chemical/drug absorption, water evaporation, deformation, and leaching of un-crosslinked reagents (van Meer et al., 2017; Toepke and Beebe, 2006; Berthier et al., 2012; Carter et al., 2020), PDMS-based MPSs have limited applications owing to the undesired influence of the cellular responses (Kamei et al., 2013). In particular, to establish *in vitro* NAFLD models, the absorption of hydrophobic molecules is considered a critical property because the key molecules for NAFLD modeling, such as free fatty acids (FFAs), are absorbed into the PDMS material to reduce the amount of hydrophobic molecules in the cell culture media (van Meer et al., 2017; Berthier et al., 2012). Moreover, PDMS absorption also reduces the tested drugs/chemicals in cell culture media, thereby causing misleading results on drug efficacy and toxicity. Therefore, there is a need for alternative materials for *in vitro* NAFLD modeling.

To fulfill these requirements, cyclo-olefin polymer (COP) has been proposed as a suitable material over PDMS because of its chemical/physical stability, high purity, and optical clarity (Campbell et al., 2020; Illa et al., 2010). Polystyrene (PS), polymethyl methacrylate (PMMA), and polypropylene (PP) are also being used as materials for cell culture plates for a long time (Campbell et al., 2020; Tsao, 2016; Puza et al., 2017; Yi et al., 2008; Nunes et al., 2010; Sun et al., 2019). However, PS and PMMA have a stronger autofluorescence compared with that of COP (Tsao and DeVoe, 2009), and PP is not as transparent as the others and therefore not suitable for cell observation (Tsao and DeVoe, 2009). Thus, COP is advantageous over PS, PMMA, and PP for applications in MPS development. Moreover, COP materials have thermostability and high modulus for metal molding processes and can be applied to mass produce MPSs. Although the previously reported microfluidic devices made of COP require solvents or adhesive tapes to assemble the COP materials, which may affect cellular phenotypes (Wan et al., 2017), the photobonding process using vacuum ultraviolet (VUV) from an excimer light source allows fabrication of the COP-based MPS without the use of additional solvents and adhesives (Yamanaka et al., 2021).

Herein, we introduce an *in vitro* NAFLD model with an MPS platform made of COP. We confirmed that the COP-MPS has the ability to prevent absorption of hydrophobic molecules, unlike PDMS-MPS. Therefore, after FFA treatment for hepatocyte-like cells (HLCs), we found that the cells cultured in the COP-MPS could be observed with AdipoRed fluorescent cellular lipid staining, whereas the HLCs in the PDMS-MPS could not be observed owing to the strong background signals of the AdipoRed absorbed in the PDMS material. Furthermore, HLCs in the COP-MPS show intracellular lipid accumulation, resulting in induction of apoptosis. Thus, COP-MPS promises to improve the MPS for applications in *in vitro* NAFLD modeling for investigating the mechanisms behind NAFLD initiation and progression and aiding drug discovery.

2. Materials and methods

2.1. Fabrication of COP-MPS

The COP-MPS comprises two layers of COP and eight microfluidic cell culture channels (800 μm width, 7500 μm length, 250 μm height), with a medium inlet and outlet (2 and 1 mm in diameter, respectively), and a total channel volume of 13.2 μL each (Yamanaka et al., 2021). The methods used to fabricate COP-MPS included metal molding (Fig. S1A) followed by photobonding (Fig. S1B), as described previously (Yamanaka et al., 2021). Two metal molds were used to fabricate the microfluidic structures. The COP material (Zeonex 480R, Zeon, Tokyo, Japan) was injected into the two molds individually. After removing the structured COP components from the molds, the components were irradiated with VUV from an excimer lamp source (172 nm; Ushio INC., Tokyo, Japan) at 25 °C. The component surfaces were then assembled using a heat press at <132 °C. Finally, ethylene oxide gas (Japan Gas Co. Ltd., Kanagawa, Japan) was used to decontaminate the fabricated COP-MPS.

2.2. Fabrication of PDMS-MPS

Polymethyl methacrylate (PMMA, Sumitomo Chemical Co., Ltd., Tokyo, Japan) was used for the micromilling procedure (CNC JIGBORER YBM 950V, Yasda Precision Tools K. K, Okayama, Japan) to fabricate the mold for the PDMS-MPS. Pre-PDMS (Sylgard184; A and B) was mixed at a 10:1 ratio and degassed for 1 h at 25 °C. The mixed pre-PDMS was then poured over the PMMA mold and placed in an oven at 65 °C for 2 h (Fig. S2). The solidified PDMS was then peeled off the mold and placed in an oven at 80 °C for 24 h. The surface of the PDMS was cleaned by soaking in ethanol (EtOH) and sonication. The PDMS part and a glass slide (Matsunami Glass, Osaka, Japan) were subsequently treated with VUV from an excimer lamp source (172 nm, Ushio INC.) at 25 °C and assembled at 80 °C for 2 d. Before being used for cell culture, this PDMS device was irradiated with UV radiation for decontamination.

2.3. Evaluation of absorption of free fatty acids in MPS

Palmitic acid sodium salt (PA, Nakalai Tesque, Kyoto, Japan) and oleic acid sodium salt (OA, Nakalai Tesque) were used as the FFAs in this study. The PA and OA stock solutions were individually prepared by dissolving in HepaRG medium 670 (KAC Co., Ltd., Tokyo, Japan) containing 30% (w/v) bovine serum albumin (BSA) (Sigma-Aldrich) solution at 300 μM for each sample. Fifteen microliters of the solution was applied to the channel of COP and PDMS device, and incubated at 37 °C, 5% CO_2 for 24 h. Each solution was collected after 24 h incubation, and FFA concentration was measured with EnzyChtomeTM free fatty acid assay kit (BioAssay Systems, Hayward, CA, USA). AdipoRed fluorescent dye (PT-7009, Lonza, Basel, Switzerland) was used to visualize the FFAs, and optical densities were measured with a Synergy HTX microplate reader (Biotek, Winooski, VT, United States) at 570 nm. AdipoRed original solution was diluted in phosphate-buffered saline (PBS) 40 times to be used as the working solution. The solution was incubated for 10 min at 25 °C. The fluorescence signals of the AdipoRed hydrophobic lipid fluorescent indicator [excitation 553 nm; emission 637 nm] in the tested materials were measured using a Nikon fluorescent microscope as described in "*2.11 Microscopic cell imaging*".

2.4. HepaRG cell culture in MPS

Prior to cell culture in the MPSs, approximately 15 μL of 0.1% (w/v) gelatin (BSA, Sigma-Aldrich, St. Louis, MO, USA) in distilled water was introduced into each microfluidic cell culture channel and maintained at 4 °C for over 24 h. The excess gelatin was then removed, and the coated channels were washed with fresh HepaRG medium 670. Differentiated HepaRG cells were obtained from KAC Co., Ltd., and the cells were

thawed in the HepaRG medium 670. After centrifugation, the cells were resuspended in fresh cell culture medium, and 15 μL of 8.0×10^6 cells mL^{-1} of the cell suspension was introduced into each microfluidic cell culture chamber.

2.5. Free fatty acid treatment

The OA:PA mixed solution was prepared as described in "*2.3 Evaluation of absorption of free fatty acids in MPS*". As a negative control, 0.3% (w/v) BSA in HepaRG medium 670 was used. Four hours after thawing, the platform was incubated at 37 °C in a humidified incubator for 24 h.

2.6. Staining for intracellular lipid accumulation

Lipid accumulation was visualized with an AdipoRed assay (Lonza, Basel, Switzerland) according to the manufacturer's protocol. The cells were fixed with 4% (v/v) PFA in PBS for 20 min at 25 °C. Next, approximately 15 μL of the AdipoRed assay reagent was mixed with 1 mL of PBS to obtain the AdipoRed staining solution. Then, 10 μL of this AdipoRed staining solution was introduced and incubated at 25 °C for 10 min. The chambers were washed with PBS three times and lastly with 300 nM of 4′,6-diamidino-2-phenylindole (DAPI) at 25 °C for 30 min.

2.7. ELISA for human albumin

The medium cultured with cells was collected and stored at −25 °C until further use. The concentration of albumin secreted into the medium was measured using the human albumin ELISA kit (Abcam, Cambridge, Cambridgeshire, UK, ab179887), following the manufacturer's protocol.

2.8. Cytochrome P450-Glo assay with luciferin

Fifteen microliters medium containing proluciferin IPA (Promega, Madison, WI, United States) was applied to the channels. The cells were incubated at 37 °C with 5% CO_2 for 1 h. Next, 10 μL medium containing luciferin IPA was collected from four channels and applied to 96 well plates; 40 μL P450 Glo reagent was subsequently added, incubated at 28 °C for 20 min, and elative light units were measured with a Synergy HTX microplate reader (Biotek, Winooski, VT, United States) at 28 °C.

2.9. Immunocytochemistry

Cells were fixed with 4% paraformaldehyde (Wako) in PBS for 20 min at 25 °C and then permeabilized with 0.1% Triton X-100 (MP Biomedicals, CA, USA) in PBS for 10 min at 25 °C. Subsequently, cells were blocked in blocking buffer (5% normal goat serum, Vector; 5% normal donkey serum, Wako; 3% bovine serum albumin, Sigma-Aldrich; and 0.1% Tween-20, Nacalai Tesque, Inc, Kyoto, Japan) in PBS at 4 °C for 16 h and then incubated at 4 °C for 16 h with the primary antibody (anti-human A1AT rabbit IgG, 1:500, Dako, Tokyo, Japan; and anti-human ALB mouse IgG, 1:500, R&D Systems) in blocking buffer. Cells were then incubated at 37 °C for 60 min with a secondary antibody (Alexa Fluor 488 Donkey anti-rabbit IgG, 1:1000, Jackson ImmunoResearch, PA, USA; and Alexa Fluor 647 Donkey anti-mouse IgG, 1:1000, Jackson ImmunoResearch) in blocking buffer before a final incubation with DAPI (Wako) at 25 °C for 30 min.

2.10. Staining for apoptotic cells

Annexin V staining was performed according to the product manual of Alexa Fluor 594-Annexin V conjugate (Molecular Probes, Eugene, OR). After washing with annexin-binding buffer (10 mM HEPES, pH 7.4, 140 mM NaCl, 2.5 mM $CaCl_2$), the cells were stained with the Alexa Fluor 594-Annexin V conjugate at 25 °C for 15 min. Following cell fixation with 4% (v/v) PFA in PBS at 25 °C for 15 min, the cells were incubated with 300 nM Hoechst 33258 at 25 °C for 30 min. To stain F-actin, the cells were incubated with 1:1000 phalloidin-iFlour 488 Reagent (abcam, Cambridge, UK) in PBS.

2.11. Microscopic cell imaging

The samples containing the cells were placed on the imaging stage of a Nikon ECLIPSE Ti inverted fluorescence microscope equipped with a CFI Plan Fluor 10 × /0.30 NA objective lens (Nikon, Tokyo, Japan), CCD camera (ORCA-R2; Hamamatsu Photonics, Hamamatsu City, Japan), mercury lamp (Intensilight; Nikon), XYZ automated stage (Ti–S-ER motorized stage with encoders; Nikon), and filter cubes for the fluorescence channels (DAPI, GFP, HYQ, and TRITC; Nikon).

2.12. Single-cell profiling based on microscopic images

Following the microscopy image acquisition, CellProfiler software (Broad Institute of Harvard and MIT, Version 3.1.9) was used to identify the cells using Otsu's method (McQuin et al., 2018). The fluorescence signals of the individual cells were quantified automatically. Density and box plots were then generated using R software (ver. 3.5.2; https://www.r-project.org/).

2.13. Statistical analysis

The P values were estimated by the Tukey-Kramer test using R software (ver. 3.5.2; https://www.r-project.org/).

3. Results

3.1. HepaRG cell culture in COP-MPS

One of the early steps in NAFLD progression in the liver is lipid accumulation after being delivered from the intestine. Therefore, treatment with FFAs for hepatocytes is commonly used as an *in vitro* NAFLD model in general cell culture. However, the MPS platforms made of PDMS have critical issues with absorption of hydrophobic molecules, including FFAs. In this study, we fabricated an MPS made of COP to prevent absorption of the FFAs for better establishment of an *in vitro* NAFLD model in the MPS (COP-MPS), as shown in Figs. 1A, 1B, and S1. This COP-MPS has eight microfluidic cell culture chambers with medium inlet and outlet (Fig. 1C). For comparison, an MPS made of PDMS with the same microfluidic structure was also fabricated (Fig. S2).

In terms of the hepatocytes, HepaRG cells were used in this study for their ability to proliferate at the undifferentiated stage and differentiate into functional HLCs. Differentiated HepaRG cells have also been used as cell sources for *in vitro* NAFLD models in literature (Rogue et al., 2014).

3.2. Treatment of FFAs induce lipid accumulation in HepaRG cells cultured in COP-MPS

Prior to establishing the *in vitro* NAFLD model in the MPS, differentiated HepaRG cells were introduced in both the COP- and PDMS-MPS. To induce NAFLD-like phenotypes *in vitro*, a mixture of FFAs (palmitic acid (PA; 16:0) and oleic acid (OA; 18:1), which are the most abundant in both healthy subjects and patients with NAFLD), was used (Gómez-Lechón et al., 2007; Yao et al., 2011; Jeon et al., 2021). BSA was used as the carrier for FFAs in the cell culture medium. Prior to FFA treatment, the absorption of hydrophobic molecules into the materials used for the MPS was evaluated using the AdipoRed fluorescent compound (Fig. 2). After 12 h of incubation of the MPS microfluidic channels with AdipoRed, the excess AdipoRed was rinsed with fresh cell culture medium. A strong AdipoRed fluorescence signal was observed in the PDMS-MPS, while the COP-PDMS did not demonstrate any fluorescence (Fig. 2A). In the case of the PDMS-MPS, an AdipoRed fluorescence signal was observed not only in the microfluidic channel but also in the PDMS

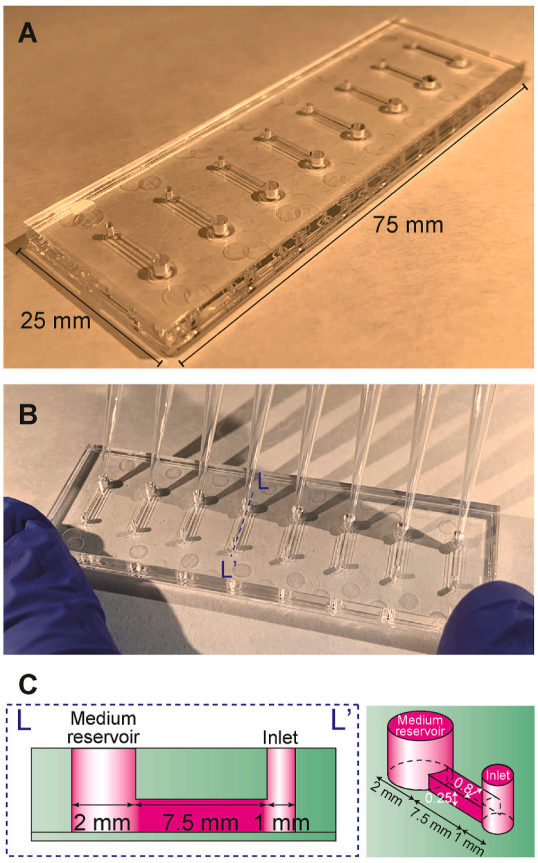

Fig. 1. (A) Photograph of a microphysiological system (MPS) made of cyclo-olefin polymer (COP), namely COP-MPS, for modeling nonalcoholic fatty liver disease (NAFLD). (B) Photograph of COP-MPS with eight tips and an octa-pipette to introduce cells and solutions into the microfluidic cell culture chambers simultaneously. (C) Schematic representation of a microfluidic cell culture chamber (L-L′) of the COP-MPS shown in (B).

material, suggesting that the AdipoRed not only covered the PDMS surface but was also absorbed into the material. According to the quantitative results based on the microscopy images shown in Fig. 2A, the COP-MPS showed very low intensity fluorescence signals within the microfluidic channel, while the PDMS-MPS showed 10.4-fold stronger fluorescence signals (Fig. 2B). We also measured the remaining FFAs in the solution after 24 h incubation with COP- and PDMS-MPS. While both OA and PA from COP-MPS remained at approximately 80%, PDMS-MPS showed significant reduction to less than 40% (Fig. 2C). These results suggested that FFAs treatment for cells cultured in PDMS-MPS did not show the proper phenotypes due to significant reductions of FFAs in the FFAs treatment solution.

Differentiated HepaRG cells were introduced into the COP- and PDMS-MPS (Fig. S3). The differentiated HepaRG cells in PDMS-MPS showed massive cell loss by medium change at 24 h after cell seeding, while the cells in COP-MPS adhered on the substrate. Then, differentiated HepaRG cells in the COP- and PDMS-MPS were treated with FFAs and stained with AdipoRed to visualize lipid accumulation in the HepaRG cells (Fig. 3). Because the PDMS-MPS absorbed the FFAs as well as AdipoRed dye, the remaining cells could not be observed clearly owing to the strong background fluorescence from the absorbed AdipoRed dye in the PDMS-MPS (Fig. 3A). Conversely, cellular lipid accumulation was observed for the COP-MPS (Fig. 3B). Therefore, the PDMS-MPS could not be used for further analyses, and only the COP-MPS was used. Treatment with FFAs (OA, PA and OA:PA) and BSA induced lipid accumulation in the differentiated HepaRG cells, and FFA treatments showed higher accumulations than that in BSA-treated HepaRG cells, as

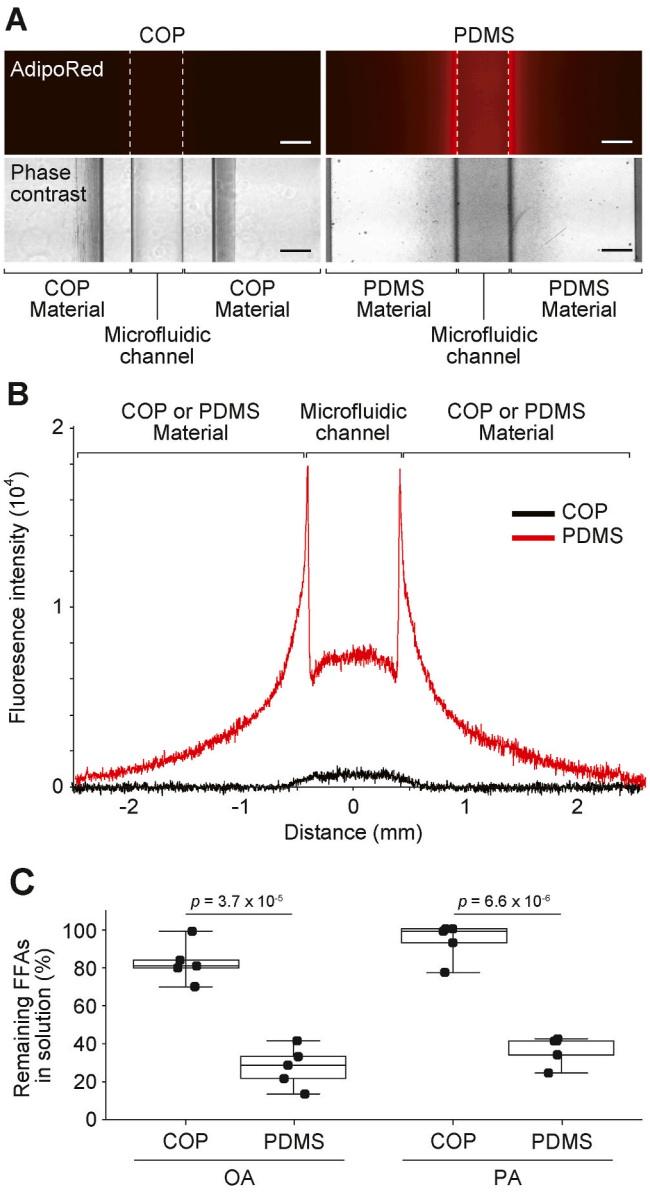

Fig. 2. Evaluation of molecular absorption into the COP and PDMS used in the MPS. (A) Micrographs of the COP- and PDMS-MPS microfluidic channels treated with AdipoRed fluorescent compound (excitation: 553 nm; emission: 637 nm) for 12 h at 25 °C. The scale bars represent 500 μm. (B) Fluorescence intensity profiles across the COP- and PDMS-MPS microfluidic channels in (A). (C) Evaluation of FFAs remaining in the solution after 24 h incubation with COP- and PDMS-MPS. The box boundaries closest and farthest from zero represent the 25th and 75th percentile, respectively. The black line within the box represents the median. The whiskers above and below the box indicate the maximum and minimum, respectively. *P* values were estimated by Student's *t*-test. All experiments were carried out at least three times.

expected.

3.3. *Accumulated lipids reduced hepatic functional protein in HepaRG cells*

To evaluate whether the accumulated lipids influence the status as a hepatocyte of HepaRG cells, we first observed the expression of α1 antitrypsin (A1AT), a hepatic maturation marker (Fig. 4), and confirmed that although A1AT protein was expressed in the treated cells (Fig. 4A), expression levels in the OA:PA treated cells were significantly reduced compared with BSA-treated cells (Fig. 4B). Moreover, we also observed

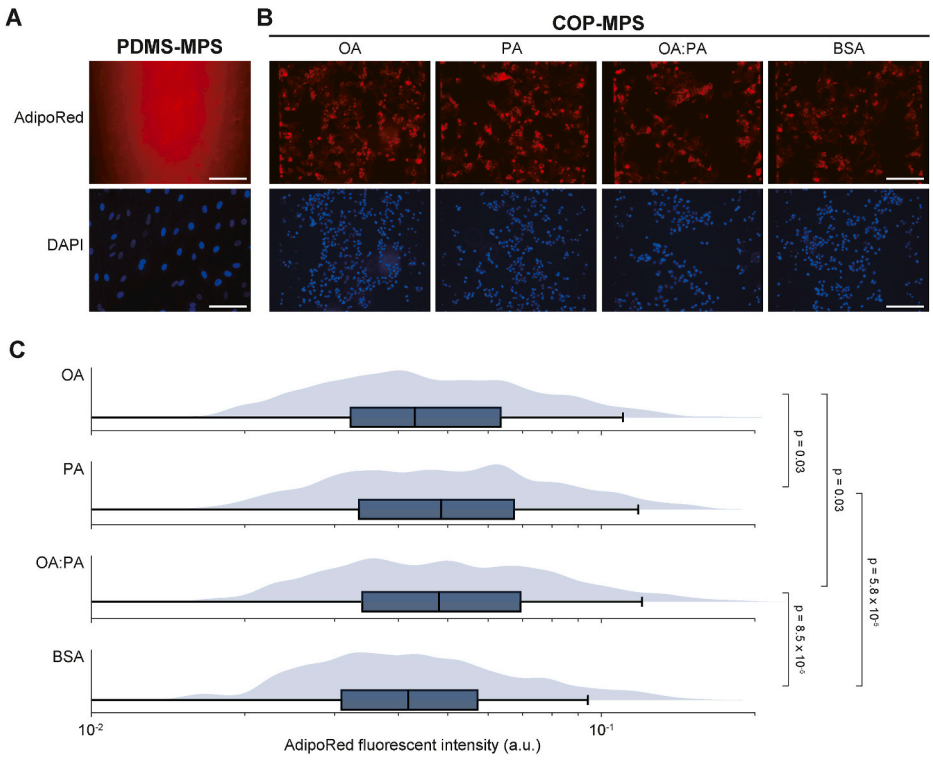

Fig. 3. Observation of lipid accumulation in HepaRG cells by AdipoRed fluorescent lipid marker. (A) Fluorescence micrographs of the HepaRG cells cultured in PDMS-MPS treated with AdipoRed dye. DAPI was used to visualize the cellular nuclei. The scale bars represent 100 μm. (B) Fluorescence micrographs of the HepaRG cells cultured in COP-MPS treated with AdipoRed dye. The scale bars represent 100 μm. (C) Density and box plots of single-cell profiles of AdipoRed fluorescence intensities of the individual FFA-treated HepaRG cells. The box boundaries closest and farthest from zero represent the 25th and 75th percentile, respectively. The black line within the box represents the median. The whiskers above and below the box indicate the maximum and minimum, respectively. Values below 10^{-2} were not shown in the graph. All experiments were carried out at least three times.

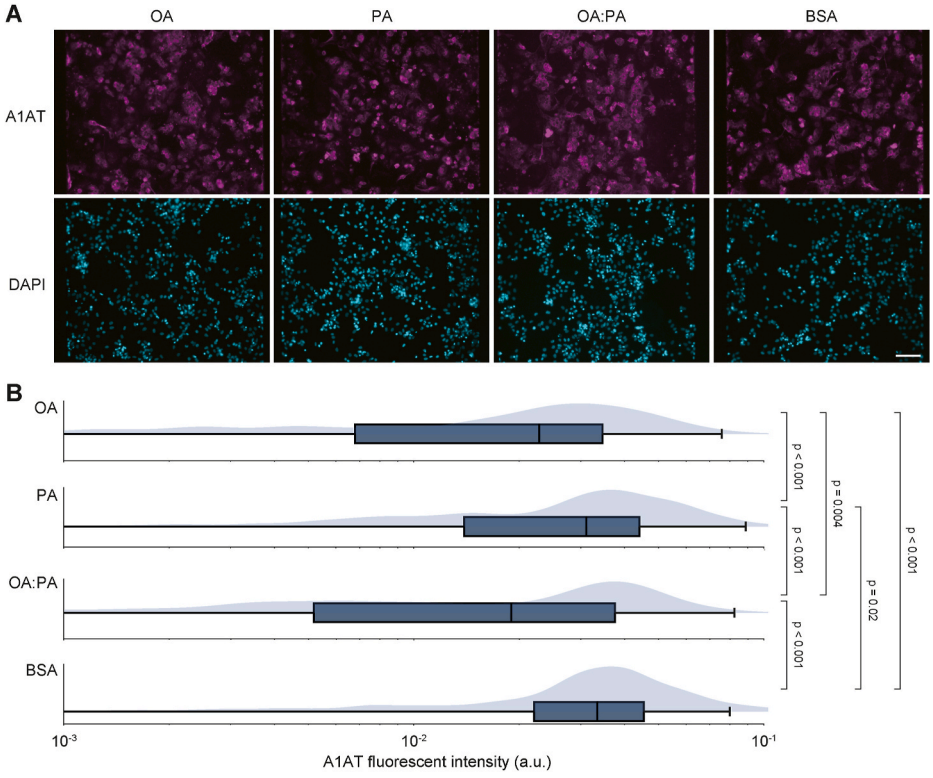

Fig. 4. Expression of α1 anti-trypsin (A1AT) protein as the hepatic maturation marker in FFAs-treated HepaRG cells cultured in COP-MPS. (A) Immunofluorescent micrographs of A1AT expression in HepaRG cells treated with OA, PA, OA:PA, and BSA. DAPI was used to stain the cell nuclei. The scale bar represents 100 μm. (B) Density and box plots of single-cell profiles of A1AT immunofluorescence intensities of individual FFAs-treated HepaRG cells in COP-MPS, based on the images shown in (A). The box boundaries closest and farthest from zero represent the 25th and 75th percentile, respectively. The black line within the box represents the median. The whiskers above and below the box indicate the maximum and minimum, respectively. Values below 10^{-3} were not shown in the graph. All experiments were carried out at least three times.

albumin (Alb) expression and secretion from FFAs-treated HepaRG cells (Fig. 5). Alb expression in FFAs-treated cells was considerably reduced compared with that in the BSA-treated cells, which was confirmed by immunocytochemistry followed by quantitative single-cell analysis (Fig. 5A and B, respectively). Secreted Alb showed a similar trend with Alb expression, but OA:PA-treated cells showed great reduction compared with solo FFA treatments (Fig. 5C). Then, we examined whether accumulated lipids influenced the hepatic metabolic activities, such as cytochrome P450 3A (CYP3A) by using bioluminescent-based CYP3A assay, and confirmed that FFA treatments reduced the CYP3A activities in HepaRG cells (Fig. 6). Taken together, FFA treatment inhibited the essential hepatic activities of HepaRG cells cultured in

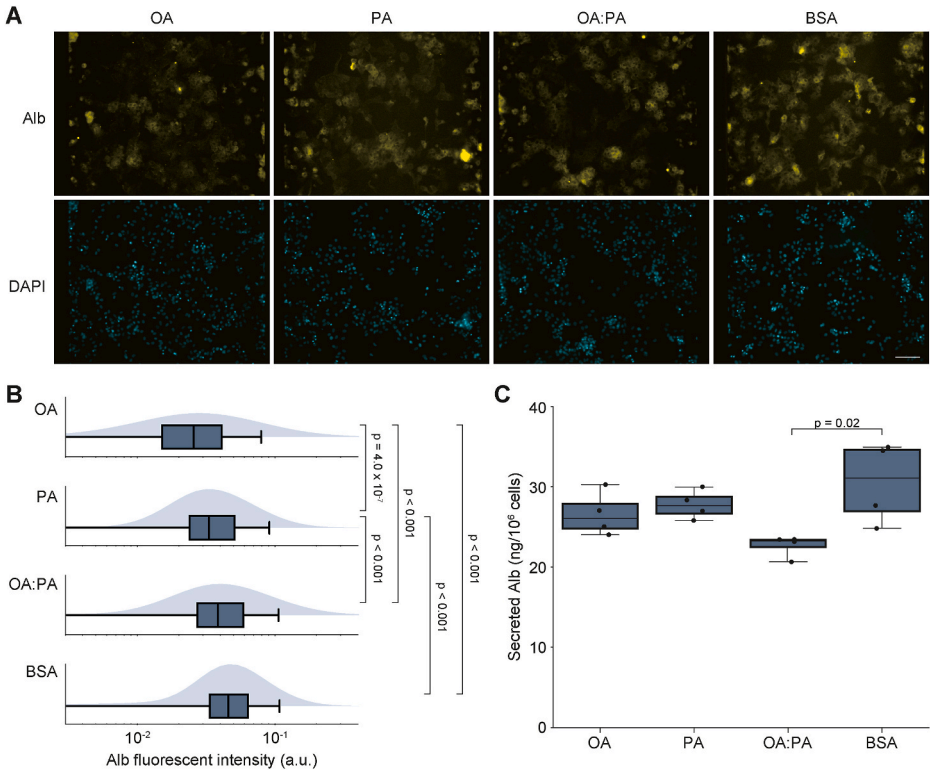

Fig. 5. Expression of human albumin (Alb) as the hepatic functional marker in FFAs-treated HepaRG cells cultured in COP-MPS. (A) Immunofluorescent micrographs of Alb expression in HepaRG cells treated with OA, PA, OA:PA and BSA. DAPI was used to stain the cell nuclei. The scale bar represents 100 μm. (B) Density and box plots of single-cell profiles of Alb immunofluorescence intensities of individual FFAs-treated HepaRG cells in COP-MPS, based on the images shown in (A). The box boundaries closest and farthest from zero represent the 25th and 75th percentile, respectively. The black line within the box represents the median. The whiskers above and below the box indicate the maximum and minimum, respectively. Values below 2×10^{-3} were not shown in the graph. (C) Secretion of Alb from in HepaRG cells treated with OA, PA, OA:PA, and BSA, determined by ELISA. The box boundaries closest and farthest from zero represent the 25th and 75th percentile, respectively. The black line within the box represents the median. The whiskers above and below the box indicate the maximum and minimum, respectively. Each dot represents each sample. All experiments were carried out at least three times.

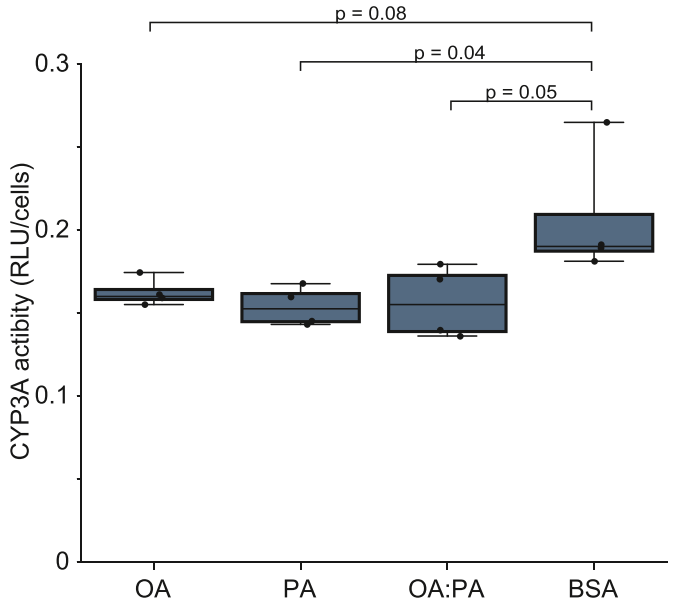

Fig. 6. Measurement of metabolic activity of cytochrome P450 3A (CYP3A) in FFAs-treated HepaRG cells cultured in COP-MPS, determined by bioluminescent-based CYP3A assay. The box boundaries closest and farthest from zero represent the 25th and 75th percentile, respectively. The black line within the box represents the median. The whiskers above and below the box indicate the maximum and minimum, respectively. Each dot represents each sample. All experiments were carried out at least three times.

COP-MPS.

3.4. *Accumulated lipids cause apoptosis of HepaRG cells cultured in COP-MPS*

To evaluate whether the accumulated lipids induced apoptosis, cellular staining with Annexin V apoptotic marker was conducted for the FFA-treated HepaRG cells in COP-MPS (Fig. 7). Regarding the fluorescence micrographs of the Annexin V stained and quantitative single-cell profiles, PA measurements for 24 h showed maximal apoptotic cells compared to other treatments, such as those with BSA and OA:PA (Fig. 4A and B). Moreover, the average nuclear size of the HepaRG cells was evaluated, as the apoptotic cells showed shrinkage of the nuclei (Fig. 4C). While the BSA- and OA:PA-treated HepaRG cells showed 656.2 ± 18.0 and 647.8 ± 11.1 μm^2, respectively, the PA-treated cells showed 553.5 ± 18.6 μm^2, showing nuclear shrinkage due to apoptosis. These results are in good agreement with the cellular lipid accumulations shown in Fig. 3, suggesting that lipid accumulation causes cellular apoptosis in HLCs.

4. Discussion

PDMS has been widely used in the fabrication of microfluidic devices, including MPS. However, PDMS usage has been associated with problems in cell culture and applications in drug development and disease modeling (van Meer et al., 2017; Toepke and Beebe, 2006; Berthier et al., 2012; Carter et al., 2020). Among these problems, absorption of the hydrophobic molecules is critical for drug development and disease modeling. Many drugs and their candidates are based on organic compounds and often have aromatic or similar structures, showing hydrophobicity. In addition, to establish an *in vitro* disease model, both genetic and chemical approaches are used, where some chemical approaches require hydrophobic molecules to recapture the pathological cellular status, e.g., FFAs for NAFLD modeling. MPS with the conventional PDMS material for NAFLD modeling has been traditionally limited by the aforementioned difficulty; thus, an alternative material is required for

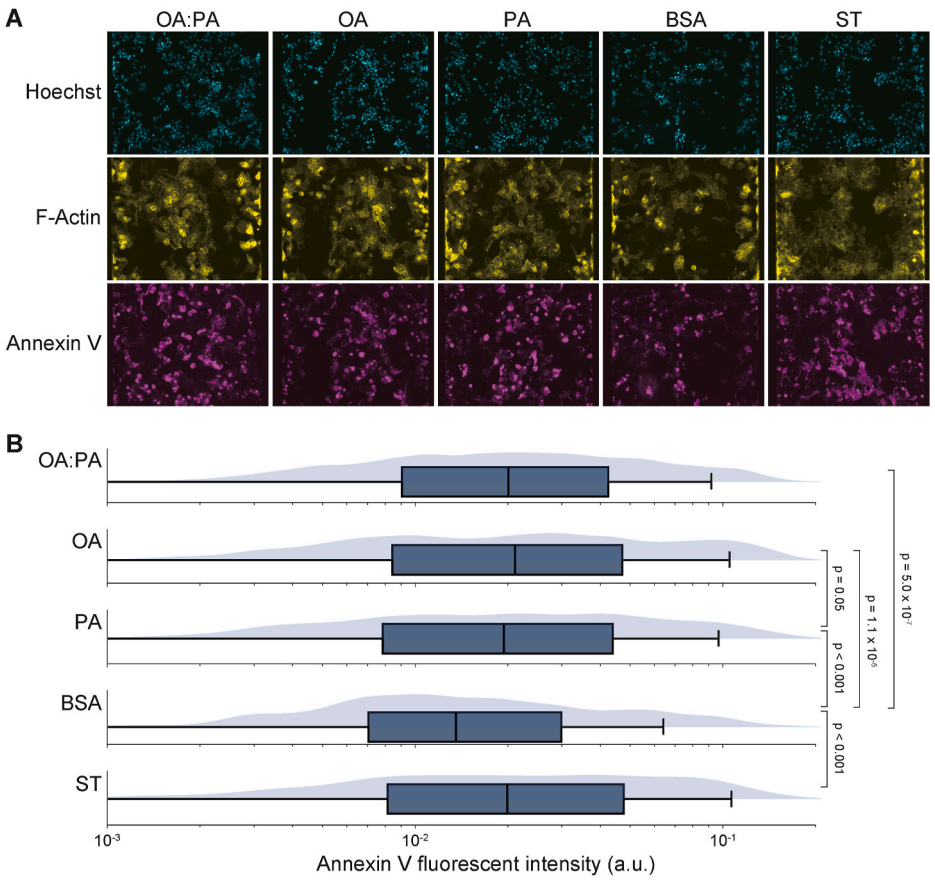

Fig. 7. Observation of apoptosis in HepaRG cells by Annexin V fluorescent apoptosis marker. (A) Fluorescence micrographs of the HepaRG cells cultured in COP-MPS stained with Annexin V to visualize apoptotic cells. Hoechst 33258 was used to visualize the cellular nuclei. F-actin was stained to visualize cytoskeleton. Staurosporine (ST) was used as a positive control of apoptotic cells. The scale bars represent 100 μm. (B) Density and box plots of single-cell profiles of Annexin V fluorescence intensities of individual FFA-treated HepaRG cells in COP-MPS, based on the images shown in (A). The box boundaries closest and farthest from zero represent the 25th and 75th percentile, respectively. The black line within the box represents the median. The whiskers above and below the box indicate the maximum and minimum, respectively. Values below 10^{-3} were not shown in the graph. All experiments were carried out at least three times.

the MPS.

To date, there have been a number of reports on the use of PDMS as an alternative to microfluidic devices for cell experiments (Berthier et al., 2012). In addition to polystyrene (PS) as the conventional material, glass, PMMA, and COP have also been tested. While glass has good optical transparency that is beneficial for observing cells, particularly for fluorescent imaging, it is too fragile for handling and microfabrication with a complicated structure. PS, PMMA, and COP are thermoplastic materials that are applicable for mass production at low costs. Because PS is known to show higher autofluorescence than PMMA and COP, it might interfere with the cellular observations during fluorescence imaging (Young et al., 2013). In the case of PMMA and COP, the solvent bonding process is required for fabrication of the microfluidic devices, and this process might disrupt the microfluidic structure (Ng et al., 2016; Shah et al., 2006) as well as cause leakage from the used solvents, thus causing cellular damage (Wan et al., 2017). PMMA also has issues with generating clacking after alcohol treatments (ethanol or isopropanol) for sterilization prior to use in cell culture. Recently, we established the COP-MPS with a photobonding process instead of solvent bonding to eliminate the drawbacks of the conventional MPS using thermoplastic materials (Yamanaka et al., 2021). This COP-MPS allows culturing of human induced pluripotent stem cells (hiPSCs) (Yu et al., 2007; Takahashi et al., 2007) and reducing undesired apoptotic cells. Thus, our proposed COP-MPS is advantageous for establishing the *in vitro* NAFLD model over the conventional MPS made of glass and other thermoplastic materials with solvent bonding.

In terms of the cell sources, HepaRG cells were used in this study as they are widely used for *in-vitro* NAFLD modeling. Nevertheless, to obtain physiologically relevant insights, primary human hepatocytes (PHHs) are still the gold standard; however, they are difficult to obtain from healthy donors and have limited proliferation. Therefore, other alternatives are utilized, and hiPSCs can be considered as potential candidates owing to their ability for unlimited self-renewal and differentiation to almost any type of tissue. Recently, there have been efforts to apply hiPSC-derived HLCs for pharmaceutical research and disease modeling (Takayama et al., 2018; Bin Ramli et al., 2020; Tian et al., 2016; Rowe and Daley, 2019; Avior et al., 2016). Using hiPSCs, three-dimensional cell culture and organoid generation with better functionalities than those of two-dimensionally cultured hepatocytes (Takayama et al., 2018; Kamei et al., 2019) can be conducted for applications to *in vitro* NAFLD modeling.

Moreover, the symptoms of NAFLD not only manifest in the liver but also in other tissues, such as the intestines and heart. These organs affect each other via the blood stream and thereby affect progression. For example, the gut–liver axis is one of the most important components for initiation and progression of NAFLD (Wiest et al., 2017; Sumida and Yoneda, 2018). To elucidate the mechanisms of NAFLD and determine the optimal treatment, such interactions need to be considered. The cell lines and primary cells are difficult to obtain from a single donor, and observation of the interactions of tissue cells from different donors might lead to incorrect results. The use of hiPSCs allows the preparation of multiple tissue cells from the same cell source, and MPS allows recapturing intertissue interactions (Kamei et al., 2017; Trapecar et al., 2020). FFAs act as the mediators of intertissue interactions, and our proposed COP-MPS would be beneficial for observing such interactions without losing the mediators for advancements in *in vitro* NAFLD modeling.

5. Conclusion

NAFLD is a critical step in the progression of liver disease and requires an *in vitro* model to understand the *in vivo* pathological conditions for drug discovery. To establish an *in vitro* NAFLD model, instead of PDMS-MPS, a COP-MPS was proposed and utilized to prevent absorption of FFAs, NAFLD initiators, and AdipoRed fluorescent lipid dye. In light

of these results, the COP-MPS has been proved to offer advantages over the PDMS-MPS, especially to establish the *in vitro* NAFLD model. To induce NAFLD-like phenotypes in differentiated HepaRG cells, PA and OA:PA were applied to the COP-MPS, and lipid accumulation was observed in the PA-treated HepaRG cells. To investigate whether the accumulated lipids caused apoptosis, Annexin V apoptotic marker staining was carried out, and it was confirmed that the PA-treated HepaRG cells had the highest rates of apoptotic cells compared to other treatments. Thus, we demonstrated an *in vitro* NAFLD model using COP-MPS. We envision that this model would be applied to drug discovery for the treatment of NAFLD, resulting in reduction of the number of liver transplants and patients with liver diseases.

Declaration of competing interest

M.Y. is an employee of Ushio Inc. A portion of this project was financially supported by Ushio Inc. The other authors declare no competing interests.

Acknowledgment

This work was supported by the Japan Society for the Promotion of Science (JSPS: 16K14660, 17H02083, and 21H01728) and the LiaoNing Revitalization Talents Program (XLYC1902061). The WPI-iCeMS is supported by the World Premier International Research Center Initiative (WPI), MEXT, Japan.

Appendix A. Supplementary data

Supplementary data to this article can be found online at https://doi.org/10.1016/j.ooc.2021.100010.

References

Avior, Y., Sagi, I., Benvenisty, N., 2016. Pluripotent stem cells in disease modelling and drug discovery. Nat. Rev. Mol. Cell Biol. 17, 170–182. https://doi.org/10.1038/nrm.2015.27.

Benam, K.H., Dauth, S., Hassell, B., Herland, A., Jain, A., Jang, K.-J., Karalis, K., Kim, H. J., MacQueen, L., Mahmoodian, R., Musah, S., Torisawa, Y., van der Meer, A.D., Villenave, R., Yadid, M., Parker, K.K., Ingber, D.E., 2015. Engineered in vitro disease models. Annu. Rev. Pathol. 10, 195–262. https://doi.org/10.1146/annurev-pathol-012414-040418.

Berthier, E., Young, E.W.K., Beebe, D., 2012. Engineers are from PDMS-land, biologists are from polystyrenia. Lab Chip 12, 1224. https://doi.org/10.1039/c2lc20982a.

Bin Ramli, M.N., Lim, Y.S., Koe, C.T., Demircioglu, D., Tng, W., Gonzales, K.A.U., Tan, C. P., Szczerbinska, I., Liang, H., Soe, E.L., Lu, Z., Ariyachet, C., Yu, K.M., Koh, S.H., Yaw, L.P., Jumat, N.H.B., Lim, J.S.Y., Wright, G., Shabbir, A., Dan, Y.Y., Ng, H.-H., Chan, Y.-S., 2020. Human pluripotent stem cell-derived organoids as models of liver disease. Gastroenterology 159, 1471–1486. https://doi.org/10.1053/j.gastro.2020.06.010 e12.

Boeckmans, J., Natale, A., Buyl, K., Rogiers, V., De Kock, J., Vanhaecke, T., Rodrigues, R. M., 2018. Human-based systems: mechanistic NASH modelling just around the corner? Pharmacol. Res. 134, 257–267. https://doi.org/10.1016/j.phrs.2018.06.029.

Byrne, C.D., Targher, G., 2015. NAFLD: a multisystem disease. J. Hepatol. 62, S47–S64. https://doi.org/10.1016/j.jhep.2014.12.012.

Campbell, S.B., Wu, Q., Yazbeck, J., Liu, C., Okhovatian, S., Radisic, M., 2020. Beyond polydimethylsiloxane: alternative materials for fabrication of organ-on-a-chip devices and microphysiological systems. ACS Biomater. Sci. Eng., 0c00640 https://doi.org/10.1021/acsbiomaterials.0c00640 acsbiomaterials.

Carter, S.-S.D., Atif, A.-R., Kadekar, S., Lanekoff, I., Engqvist, H., Varghese, O.P., Tenje, M., Mestres, G., 2020. PDMS leaching and its implications for on-chip studies focusing on bone regeneration applications. Organs-on-a-Chip 2, 100004. https://doi.org/10.1016/j.ooc.2020.100004.

Davidson, M.D., Ballinger, K.R., Khetani, S.R., 2016. Long-term exposure to abnormal glucose levels alters drug metabolism pathways and insulin sensitivity in primary human hepatocytes. Sci. Rep. 6, 28178. https://doi.org/10.1038/srep28178.

Gómez-Lechón, M.J., Donato, M.T., Martínez-Romero, A., Jiménez, N., Castell, J.V., O'Connor, J.-E., 2007. A human hepatocellular in vitro model to investigate steatosis. Chem. Biol. Interact. 165, 106–116. https://doi.org/10.1016/j.cbi.2006.11.004.

Illa, X., Ordeig, O., Snakenborg, D., Romano-Rodríguez, A., Compton, R.G., Kutter, J.P., 2010. A cyclo olefin polymer microfluidic chip with integrated gold microelectrodes for aqueous and non-aqueous electrochemistry. Lab Chip 10, 1254–1261. https://doi.org/10.1039/b926737a.

Jeon, J., Lee, S.H., Kim, D., Sung, J.H., 2021. In vitro hepatic steatosis model based on gut–liver-on-a-chip. Biotechnol. Prog. 37, 1–13. https://doi.org/10.1002/btpr.3121.

Kamei, K., Hirai, Y., Yoshioka, M., Makino, Y., Yuan, Q., Nakajima, M., Chen, Y., Tabata, O., 2013. Phenotypic and transcriptional modulation of human pluripotent stem cells induced by nano/microfabrication materials. Adv. Healthc. Mater. 2, 287–291. https://doi.org/10.1002/adhm.201200283.

Kamei, K., Kato, Y., Hirai, Y., Ito, S., Satoh, J., Oka, A., Tsuchiya, T., Chen, Y., Tabata, O., 2017. Integrated heart/cancer on a chip to reproduce the side effects of anti-cancer drugs in vitro. RSC Adv. 7, 36777–36786. https://doi.org/10.1039/C7RA07716E.

Kamei, K., Yoshioka, M., Terada, S., Tokunaga, Y., Chen, Y., 2019. Three-dimensional cultured liver-on-a-Chip with mature hepatocyte-like cells derived from human pluripotent stem cells, Biomed. Microdevices 21, 73. https://doi.org/10.1007/s10544-019-0423-8.

Kimura, H., Sakai, Y., Fujii, T., 2018. Organ/body-on-a-chip based on microfluidic technology for drug discovery. Drug Metabol. Pharmacokinet. 33, 43–48. https://doi.org/10.1016/j.dmpk.2017.11.003.

Liu, Y., Meyer, C., Xu, C., Weng, H., Hellerbrand, C., ten Dijke, P., Dooley, S., 2013. Animal models of chronic liver diseases. AJP Gastrointest. Liver Physiol. 304, G449–G468. https://doi.org/10.1152/ajpgi.00199.2012.

McQuin, C., Goodman, A., Chernyshev, V., Kamentsky, L., Cimini, B.A., Karhohs, K.W., Doan, M., Ding, L., Rafelski, S.M., Thirstrup, D., Wiegraebe, W., Singh, S., Becker, T., Caicedo, J.C., Carpenter, A.E., 2018. CellProfiler 3.0: next-generation image processing for biology. PLoS Biol. 16, e2005970 https://doi.org/10.1371/journal.pbio.2005970.

Ng, S.P., Wiria, F.E., Tay, N.B., 2016. Low distortion solvent bonding of microfluidic chips. Procedia Eng. 141, 130–137. https://doi.org/10.1016/j.proeng.2015.09.212.

Nunes, P.S., Ohlsson, P.D., Ordeig, O., Kutter, J.P., 2010. Cyclic olefin polymers: emerging materials for lab-on-a-chip applications. Microfluid. Nanofluidics 9, 145–161. https://doi.org/10.1007/s10404-010-0605-4.

Puza, S., Gencturk, E., Odabasi, I.E., Iseri, E., Mutlu, S., Ulgen, K.O., 2017. Fabrication of cyclo olefin polymer microfluidic devices for trapping and culturing of yeast cells. Biomed. Microdevices 19, 40. https://doi.org/10.1007/s10544-017-0182-3.

Rogue, A., Anthérieu, S., Vluggens, A., Umbdenstock, T., Claude, N., de la Moureyre-Spire, C., Weaver, R.J., Guillouzo, A., 2014. PPAR agonists reduce steatosis in oleic acid-overloaded HepaRG cells. Toxicol. Appl. Pharmacol. 276, 73–81. https://doi.org/10.1016/j.taap.2014.02.001.

Rowe, R.G., Daley, G.Q., 2019. Induced pluripotent stem cells in disease modelling and drug discovery. Nat. Rev. Genet. 1. https://doi.org/10.1038/s41576-019-0100-z.

Shah, J.J., Geist, J., Locascio, L.E., Gaitan, M., Rao, M.V., Vreeland, W.N., 2006. Capillarity induced solvent-actuated bonding of polymeric microfluidic devices. Anal. Chem. 78, 3348–3353. https://doi.org/10.1021/ac051883l.

Soto-Gutierrez, A., Gough, A., Vernetti, L.A., Taylor, D.L., Monga, S.P., 2017. Pre-clinical and clinical investigations of metabolic zonation in liver diseases: the potential of microphysiology systems. Exp. Biol. Med. 242, 1605–1616. https://doi.org/10.1177/1535370217707731.

Sumida, Y., Yoneda, M., 2018. Current and future pharmacological therapies for NAFLD/NASH. J. Gastroenterol. 53, 362–376. https://doi.org/10.1007/s00535-017-1415-1.

Sun, H., Chan, C.-W., Wang, Y., Yao, X., Mu, X., Lu, X., Zhou, J., Cai, Z., Ren, K., 2019. Reliable and reusable whole polypropylene plastic microfluidic devices for a rapid, low-cost antimicrobial susceptibility test. Lab Chip 19, 2915–2924. https://doi.org/10.1039/C9LC00502A.

Sung, J.H., Wang, Y.I., Narasimhan Sriram, N., Jackson, M., Long, C., Hickman, J.J., Shuler, M.L., 2019. Recent advances in body-on-a-chip systems. Anal. Chem. 91, 330–351. https://doi.org/10.1021/acs.analchem.8b05293.

Takahashi, K., Tanabe, K., Ohnuki, M., Narita, M., Ichisaka, T., Tomoda, K., Yamanaka, S., 2007. Induction of pluripotent stem cells from adult human fibroblasts by defined factors. Cell 131, 861–872. https://doi.org/10.1016/j.cell.2007.11.019.

Takayama, K., Hagihara, Y., Toba, Y., Sekiguchi, K., Sakurai, F., Mizuguchi, H., 2018. Enrichment of high-functioning human iPS cell-derived hepatocyte-like cells for pharmaceutical research. Biomaterials 161, 24–32. https://doi.org/10.1016/j.biomaterials.2018.01.019.

Tian, L., Prasad, N., Jang, Y.-Y., 2016. In vitro modeling of alcohol-induced liver injury using human-induced pluripotent stem cells. Methods Mol. Biol. 1353, 271–283. https://doi.org/10.1007/7651_2014_168.

Tilg, H., Adolph, T.E., Moschen, A.R., 2020. Multiple parallel hits hypothesis in NAFLD – revisited after a decade. Hepatology. https://doi.org/10.1002/hep.31518 hep.31518.

Toepke, M.W., Beebe, D.J., 2006. PDMS absorption of small molecules and consequences in microfluidic applications. Lab Chip 6, 1484. https://doi.org/10.1039/b612140c.

Trapecar, M., Communal, C., Velazquez, J., Maass, C.A., Huang, Y.-J., Schneider, K., Wright, C.W., Butty, V., Eng, G., Yilmaz, O., Trumper, D., Griffith, L.G., 2020. Gut-liver physiomimetics reveal paradoxical modulation of IBD-related inflammation by short-chain fatty acids. Cell Syst. 10, 223–239. https://doi.org/10.1016/j.cels.2020.02.008 e9.

Tsao, C.-W., 2016. Polymer microfluidics: simple, low-cost fabrication process bridging academic lab research to commercialized production. Micromachines 7, 225. https://doi.org/10.3390/mi7120225.

Tsao, C.-W., DeVoe, D.L., 2009. Bonding of thermoplastic polymer microfluidics. Microfluid. Nanofluidics 6, 1–16. https://doi.org/10.1007/s10404-008-0361-x.

van Meer, B.J., de Vries, H., Firth, K.S.A., van Weerd, J., Tertoolen, L.G.J., Karperien, H. B.J., Jonkheijm, P., Denning, C., IJzerman, A.P., Mummery, C.L., 2017. Small molecule absorption by PDMS in the context of drug response bioassays. Biochem. Biophys. Res. Commun. 482, 323–328. https://doi.org/10.1016/j.bbrc.2016.11.062.

Wan, A.M.D., Moore, T.A., Young, E.W.K., 2017. Solvent bonding for fabrication of PMMA and COP microfluidic devices. JoVE 119, e55175. https://doi.org/10.3791/55175.

Wiest, R., Albillos, A., Trauner, M., Bajaj, J.S., Jalan, R., 2017. Targeting the gut-liver axis in liver disease. J. Hepatol. 67, 1084–1103. https://doi.org/10.1016/j.jhep.2017.05.007.

Yamanaka, M., Wen, X., Imamura, S., Sakai, R., Terada, S., Kamei, K., 2021. Cyclo olefin polymer-based solvent-free mass-productive microphysiological systems. Biomed. Mater. 1–11. https://doi.org/10.1088/1748-605X/abe660.

Yao, H.-R., Liu, J., Plumeri, D., Cao, Y.-B., He, T., Lin, L., Li, Y., Jiang, Y.-Y., Li, J., Shang, J., 2011. Lipotoxicity in HepG2 cells triggered by free fatty acids. Am. J. Transl. Res. 3, 284–291. http://www.ncbi.nlm.nih.gov/pubmed/21654881%0Ahttp://www.pubmedcentral.nih.gov/articlerender.fcgi?artid=PMC3102573.

Yi, L., Xiaodong, W., Fan, Y., 2008. Microfluidic chip made of COP (cyclo-olefin polymer) and comparion to PMMA (polymethylmethacrylate) microfluidic chip. J. Mater. Process. Technol. 208, 63–69. https://doi.org/10.1016/J.JMATPROTEC.2007.12.146.

Young, E.W.K., Berthier, E., Beebe, D.J., 2013. Assessment of enhanced autofluorescence and impact on cell microscopy for microfabricated thermoplastic devices. Anal. Chem. 85, 44–49. https://doi.org/10.1021/ac3034773.

Younossi, Z.M., 2019. Non-alcoholic fatty liver disease – a global public health perspective. J. Hepatol. 70, 531–544. https://doi.org/10.1016/j.jhep.2018.10.033.

Younossi, Z., Tacke, F., Arrese, M., Chander Sharma, B., Mostafa, I., Bugianesi, E., Wai-Sun Wong, V., Yilmaz, Y., George, J., Fan, J., Vos, M.B., 2019. Global perspectives on nonalcoholic fatty liver disease and nonalcoholic steatohepatitis. Hepatology 69, 2672–2682. https://doi.org/10.1002/hep.30251.

Yu, J., Vodyanik, M.A., Smuga-Otto, K., Antosiewicz-Bourget, J., Frane, J.L., Tian, S., Nie, J., Jonsdottir, G.A., Ruotti, V., Stewart, R., Slukvin, I.I., Thomson, J.A., 2007. Induced pluripotent stem cell lines derived from human somatic cells. Science 318, 1917–1920. https://doi.org/10.1126/science.1151526, 80-.